
This is an electronic reprint of the original article.
This reprint may differ from the original in pagination and typographic detail.

Malitckii, Evgenii; Yagodzinskyy, Yuriy; Vilaça, Pedro

Role of retained austenite in hydrogen trapping and hydrogen-assisted fatigue fracture of high-strength steels

Published in:
Materials Science and Engineering A

DOI:
[10.1016/j.msea.2019.05.103](https://doi.org/10.1016/j.msea.2019.05.103)

Published: 08/07/2019

Document Version
Publisher's PDF, also known as Version of record

Published under the following license:
CC BY-NC-ND

Please cite the original version:
Malitckii, E., Yagodzinskyy, Y., & Vilaça, P. (2019). Role of retained austenite in hydrogen trapping and hydrogen-assisted fatigue fracture of high-strength steels. *Materials Science and Engineering A*, 760, 68-75. <https://doi.org/10.1016/j.msea.2019.05.103>

This material is protected by copyright and other intellectual property rights, and duplication or sale of all or part of any of the repository collections is not permitted, except that material may be duplicated by you for your research use or educational purposes in electronic or print form. You must obtain permission for any other use. Electronic or print copies may not be offered, whether for sale or otherwise to anyone who is not an authorised user.



Role of retained austenite in hydrogen trapping and hydrogen-assisted fatigue fracture of high-strength steels

Evgenii Malitskii*, Yuriy Yagodzinsky, Pedro Vilaça

Aalto University, School of Engineering, Department of Mechanical Engineering, Espoo, Finland



ARTICLE INFO

Keywords:

High-strength steel
Retained austenite
Hydrogen embrittlement
Fatigue

ABSTRACT

The Interaction of hydrogen with retained austenite under fatigue loading of dual-phase and complex-phase high-strength steels with strength of about 1200 MPa was studied. A load-controlled fatigue test was performed in the air with the maximum applied tensile strength of 900 MPa, which is just below the offset yield point of the studied steels. The trapping of hydrogen accumulated into the studied steels under the fatigue loading was studied by thermal desorption spectroscopy. Measurements of hydrogen trapping evolution and microstructure changes during fatigue testing reveal a complicated hydrogen trapping behavior driven by hydrogen interaction with deformation defects and retained austenite. Hydrogen concentration increases in the studied steels during the fatigue testing in the air without preceding hydrogen charging. The fracture surfaces were studied by scanning electron microscopy evidencing the relationship between the hydrogen concentration increase related to retained austenite and initiation of the intergranular fatigue fracture. The role of retained austenite in hydrogen-assisted fatigue cracking is discussed and a possible mechanism of the hydrogen-assisted fatigue crack initiation in the high-strength steels is proposed.

1. Introduction

The use of advanced high-strength steels (HSS) in the transport industry is a promising way to significantly reduce the weight of the products, improve the fuel economy and reduce emissions into the atmosphere. However, HSS grades are sensitive to hydrogen embrittlement even at a relatively low hydrogen concentration [1,2]. At the same time, the morphology of hydrogen-assisted fracture in high-strength steel depends significantly on the steel microstructure [3–10]. The interaction of hydrogen with phase constituents of HSS leading to hydrogen embrittlement is a key problem of these materials.

In HSS with increased hydrogen concentration caused by hydrogen charging non-metallic inclusions (NMI) play an important role in hydrogen embrittlement [3–5]. Hydrogen interaction with NMIs facilitates crack initiation in HSS grades. For example, the alloying of the steel with Ti results in the formation of transgranular hydrogen-induced cracks initiated at Ti-based non-metallic inclusions during constant extension rate tensile testing [3]. It was assumed also that crack initiation and propagation in HSS under fatigue loading is related to hydrogen trapping by NMIs [4]. However, in HSS with low Ti content the hydrogen-induced fracture is a complex mixture of inter- and transgranular brittle facets with a number of secondary cracks [5]. One can assume that the intergranular cracking and secondary cracks

formation are the main attributes of the hydrogen-assisted cracking in HSS grades, which consist of a minor amount of NMIs.

Increased hydrogen concentration caused by hydrogen charging of HSS results in a significant change of the fracture morphology [3,4,6,7]. However, the effect of the minor hydrogen concentration accumulated during the steel processing or exploitation is still unclear. Secondary cracks were observed in HSS tested under fatigue loading in the air. Sudhakar et al. [6] reported the formation of the transgranular fracture surface with secondary cracks in dual-phase high-strength steel. It was shown that the amount of the secondary cracks increases with increase of the martensite content in the HSS [4]. The effect of the stress intensity factor on the secondary cracks formation has been studied by Onn et al. [7], who associated the extensive secondary cracking with high mean stress level of the fatigue loading. At the same time, both authors proposed the hydrogen embrittlement as the possible reason for the origin of the observed secondary cracks. Intergranular cracking has been also observed in high-strength steels after fatigue loading in the air. Fracture morphology of tempered HSSs exhibits a fracture partially transgranular faceted and partially intergranular [3]. The formation of intergranular fracture was found to be dependent on the stress intensity factor and attributed to the mechanism of dislocation pile-up forming along slip planes and providing the hydrogen transport to the grain boundaries [8].

* Corresponding author.

E-mail address: evgeny.malitskiy@aalto.fi (E. Malitskii).

<https://doi.org/10.1016/j.msea.2019.05.103>

Received 2 October 2018; Received in revised form 25 April 2019; Accepted 28 May 2019

Available online 29 May 2019

0921-5093/ © 2019 The Authors. Published by Elsevier B.V. This is an open access article under the CC BY-NC-ND license (<http://creativecommons.org/licenses/by-nc-nd/4.0/>).

Retained austenite (RA) that is always present in the multiphase HSS grades may act as a considerable trapping site of hydrogen. The role of the RA in hydrogen trapping has been studied by Chan et al. [9] evidencing an increase of hydrogen concentration with an increase of the retained austenite content in martensitic steel after hydrogen charging. The deleterious effect of hydrogen on the ductility of supermartensitic stainless steel increases significantly in the presence of the retained austenite as shown by Solheim [10]. The presence of the retained austenite undoubtedly facilitates the hydrogen embrittlement in high-strength steels, but its role and detailed mechanism in hydrogen transport and trapping during fatigue loading remains unclear.

The objective of the present research is to investigate the role of retained austenite in hydrogen trapping and hydrogen-assisted cracking under fatigue loading in the air, without hydrogen pre-charging. Other research questions addressed in this study are the redistribution of the hydrogen trapped in retained austenite during its transformation caused by fatigue loading [11,12] and/or hydrogen accumulation from the air environment [13]. Despite the fact that the effect of hydrogen on fatigue has been extensively studied for a variety of the materials, the phenomena of hydrogen uptake under fatigue loading, where fatigue loading is the driving force for the hydrogen uptake, has never been studied in detail, especially for modern HSS grades. Even a minor increase of hydrogen concentration in HSS under fatigue loading may facilitate fatigue crack initiation and growth [14]. The present paper investigates and reveals the phenomena of the hydrogen uptake in HSS under fatigue loading and the correlation between the microstructural change and hydrogen trapping providing valuable incremental knowledge on hydrogen behavior and distribution in HSS.

2. Experimental

Two high-strength steel grades of the same chemical composition, but different heat treatment were supplied by voestalpine AG in form of 1 mm thick plates. The chemical composition of the steels is shown in Table 1. The microstructure of the steels was a dual phase (DP) consisting of about 50% ferrite and 50% martensite and a complex phase (CP) consisting of martensite, tempered martensite, bainite, and ferrite phases. The steels also contain a different amount of the retained austenite found to be about 1.3% and 6.3% for DP and CP steel grades, respectively. Quantitative measurements of the RA volume fraction were performed using magnetic analysis [3]. The mechanical properties, microstructure and heat treatment procedures related to the studied DP and CP steels are described in details by Hickel et al. [3], where DP and CP steels are corresponding to the grades VA-1200-M05 and VA-1200-MTM, respectively. Steel plates were cut using electrical discharge machining (EDM) in the specimens of sub-sized shape with the gauge length of about 20 mm and 4 mm width as shown in Fig. 1.

Gauge parts of the specimens were mechanically polished finishing with No. 2500 emery paper. Constant extension rate tests (CERT) were performed with the strain rate of 10^{-4} s^{-1} using electromechanical 30 kN MTS. Typical stress-strain curves of both steels are shown in Fig. 2. Fatigue loading was performed in air using a servo-hydraulic MTS 858 tabletop system, where the specimen was subjected to uniaxial cyclic loading with $\sigma_{\max} = 900 \text{ MPa}$, $R = 0$, and the fatigue frequency of 12 Hz. The maximum applied stress was chosen to be less than the offset yield point for both studied steels. Fatigue life (N_f) was found to be about 15 000 cycles and 50 000 cycles for DP and CP steels, respectively. The fatigue testing program was defined choosing the

Table 1

Chemical composition of the studied steels with different heat treatment leading to DP and CP structure (wt.%).

C	Si	Mn	Al	Ti	Cr	N	S
0.157	0.19	2.24	0.053	0.002	0.46	0.006	0.001

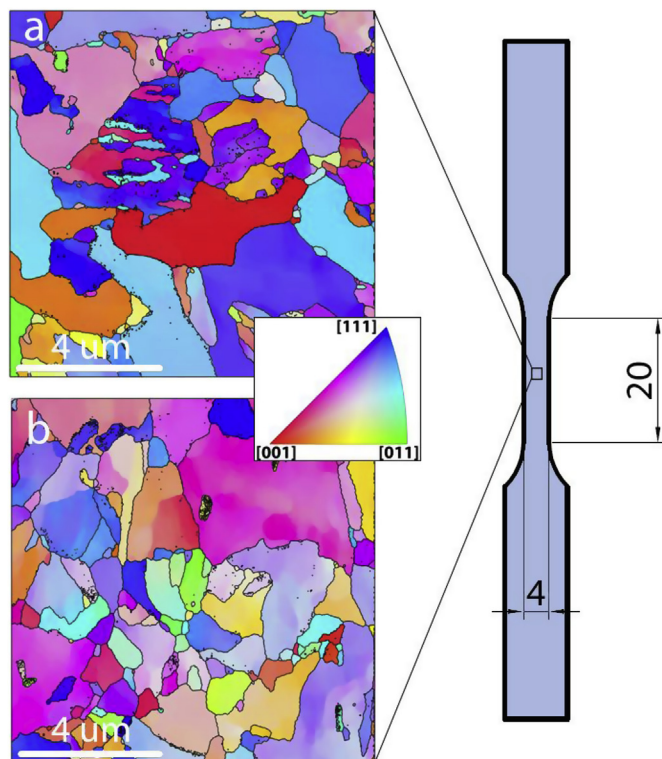


Fig. 1. Schematic view of the fatigue specimen. Inverse pole figure (IPF) maps of the studied DP (a) and CP (b) HSS grades.

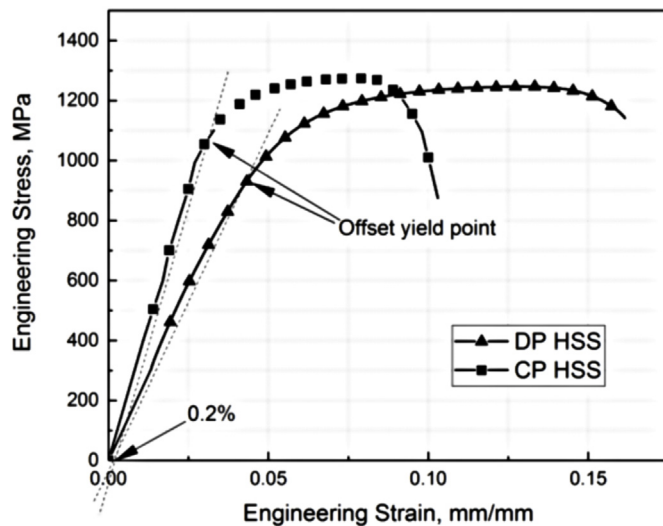


Fig. 2. CERT stress-strain curves of the studied HSS grades. Strain rate 10^{-4} s^{-1} .

Table 2

Fatigue testing program.

Material	Number of cycles			
DP HSS	100	1000	3000	$N_f = 15\ 000$
CP HSS	5000	20 000	40 000	$N_f = 50\ 000$

intermediate number of the fatigue cycles as shown in Table 2.

Hydrogen uptake and trapping were analyzed in both steels after a particular number of the loading cycles listed in Table 2. Hydrogen thermal desorption spectroscopy (TDS) measurements were performed at temperatures from RT to 1000 K with the heating rate of 6 K/min for

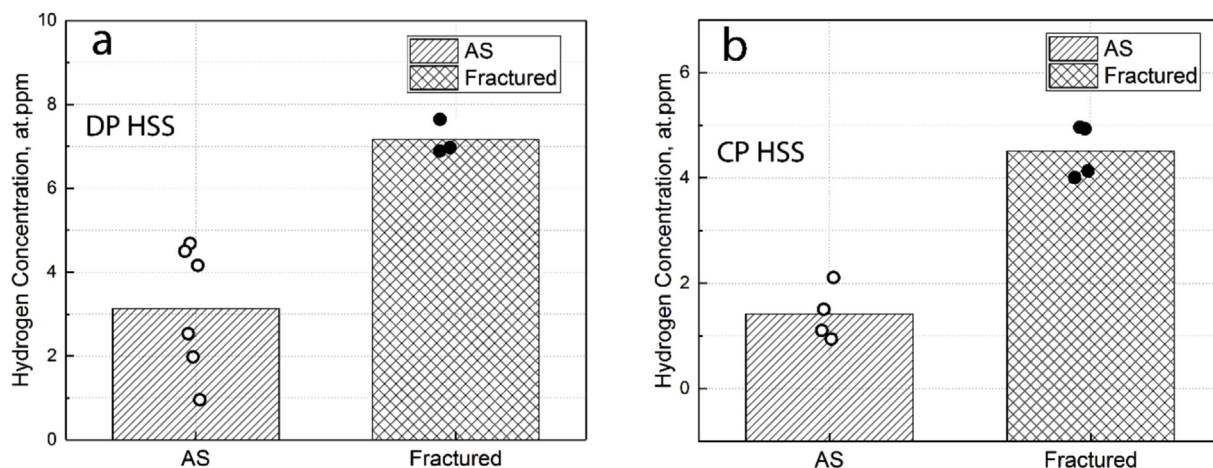


Fig. 3. Hydrogen concentration in DP (a) and CP (b) steels in as-supplied state (AS) and after fatigue failure.

the specimens in as-supplied condition and after interrupted fatigue loading as well as after specimen fracture.

Microstructural changes of the steels were controlled by electron backscatter diffraction (EBSD) analysis. EBSD samples were cut from the gauge part of the tested specimens and polished finishing with 0.02 μm colloidal silica. The side surface of the specimens was exposed for EBSD analysis as shown in Fig. 1. MTEX toolbox for MATLAB software was used for EBSD data processing.

3. Results

Thermal desorption measurements were performed for specimens in the as-supplied state and after fatigue testing. In the as-supplied state the average hydrogen concentration was measured to be about 3.1 at ppm and 1.4 at ppm in the DP and CP steels, respectively (see Fig. 3a and b). It is notable that the hydrogen concentration measured for a set of as-supplied samples manifests a broad distribution, especially in DP steel.

TDS measurements performed for fatigue tested specimens reveal a significant increase in hydrogen concentration. The increase was found to be about 7.3 at ppm and 4.5 at ppm in the DP and CP steels, respectively. Fatigue loading in air results in hydrogen uptake that increases the total hydrogen concentration at about two times in DP HSS and at about three times in CP HSS. It should be noted also, that duration of the fatigue testing in the CP steel was about 3 times longer than DP steel as seen from the fatigue program of the studied steels in Table 2.

Hydrogen uptake and trapping were studied in details using thermal desorption spectroscopy analysis performed according to the program of fatigue testing shown in Table 2. TDS curves of hydrogen release from the steels shown in Fig. 4a and b have a complex shape caused by a considerable amount of the different trapping sites for hydrogen. Nevertheless, the behavior of the hydrogen desorption rates in the DP and CP HSS grades are similar. The obtained spectra have a well-defined low (from room temperature (RT) to 550 K) and high (from 550 K to 1000 K) components, which are characteristic for both studied steels. The low-temperature component increases with the number of the fatigue cycles for both steels. At the same time, the high-temperature component appearance is independent of the applied fatigue loading. The hydrogen concentration was calculated using the area under the TDS curve which is equivalent to the hydrogen concentration in the steel [15,16]. Anomalous behavior of the high-temperature component results in irregular hydrogen concentration measured after a different amount of the fatigue cycles, especially in the CP steel.

Each TDS curve shown in Fig. 4a and b has a similar complex shape caused by the hydrogen trapping in the trapping sites of different origin

[17]. The complex character of trapping was analyzed assuming that a low-temperature peak consists of a few gaussian peaks, as was proposed by Smith et al. [17]. An example of the TDS curve fitting with the Gaussian components is shown in Fig. 5a and b for both steels. Best fitting was obtained using six Gaussian peaks and exponential background. It is assumed that the exponential background originates from the so-called diffusible hydrogen (DH), the desorption rate of which is rather high at room temperature and decreases exponentially with reduction of the DH concentration. As seen in Fig. 5 a, b the low-temperature component is a sum of three Gaussians with the peak at temperatures of about 420 K, 450 K and 520 K for DP steel, and 390 K, 410 K, and 500 K for CP steel.

Hydrogen concentration was calculated from the fitting data separately for each Gaussian peak. Fig. 6 shows hydrogen concentration for each component as well as their sum as a function of fatigue cycle number. The concentration of hydrogen calculated from peak 1, 2 increases under fatigue loading for 3000 cycles (see Fig. 6a). Then the hydrogen concentration calculated from peak 1 remains almost constant until the end of the fatigue life of the DP steel, while concentration associated with peak 2 decreases. Since the first peak is dominant, the total hydrogen concentration of the three peaks shown in Fig. 6b has a similar behavior approaching saturation of hydrogen concentration at about 5 at ppm after 3000 cycles. The behavior of the hydrogen uptake and trapping in the CP steel under fatigue loading for 20 000 cycles is comparable to that observed in DP steel for all fatigue life. A steep growth of hydrogen concentration related to peaks 1 and 2 was observed after fatigue loading for 5000 cycles (see Fig. 6c). However, the hydrogen concentration corresponding to peak 1 is significantly smaller (about of 1.5 at ppm) as compared to which is in the DP steel. The total hydrogen concentration (see Fig. 6d) shows the saturation range between 5000 and 20 000 cycles that is similar to the results obtained for the DP steel. After 20 000 cycles, the hydrogen concentration of the peak 2 and 3 turns to increase until the end of fatigue life of the CP steel. The hydrogen concentration of the peak 1 increases also with further fatigue loading approaching the saturation range between 40 000 and 50 000 cycles. The total hydrogen concentration (see Fig. 6d) increases continuously with a further increase of fatigue cycle to the end of the fatigue life of the CP steel.

Hydrogen uptake and trapping depend significantly on the microstructure of metallic materials. Fatigue loading may result in microstructural changes, which are responsible for the observed variation of hydrogen uptake. EBSD analysis was performed for both studied steels in as-supplied state and after fatigue loading. Phase contrast micrographs of studied steels were obtained from the EBSD data as shown in Fig. 7. Ferrite and martensite phases are shown in Fig. 7 in blue. The martensite phase is marked out by a dark tone. The retained austenite is

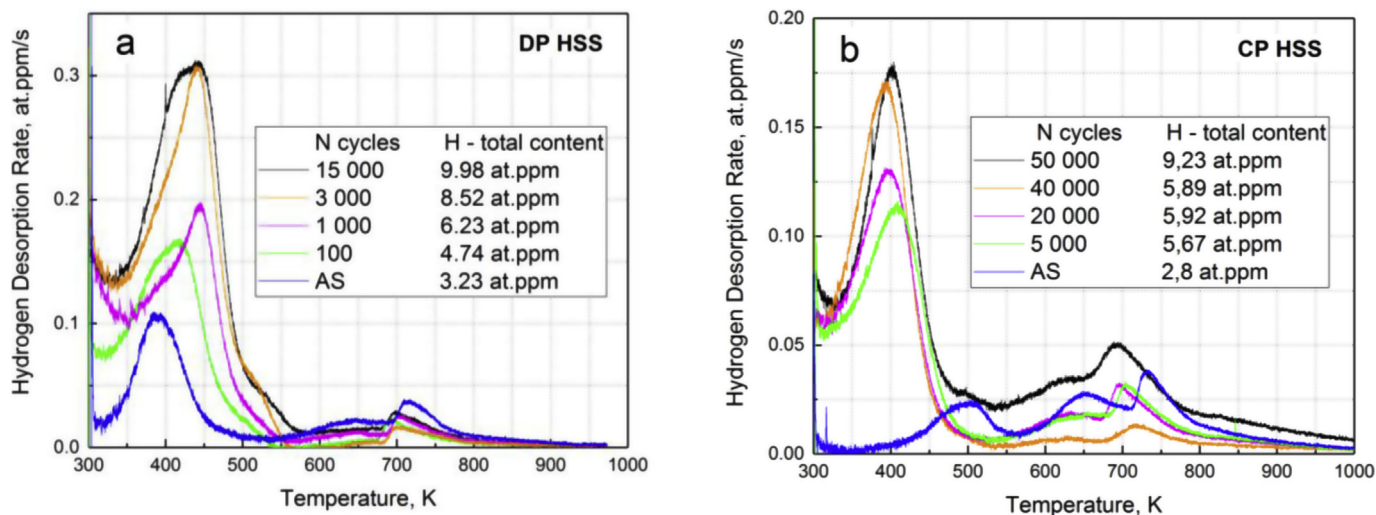


Fig. 4. TDS curves of hydrogen desorption rate from DP (a) and CP (b) steels measured in as-supplied state and after fatigue loading according to the fatigue testing program (see Table 2).

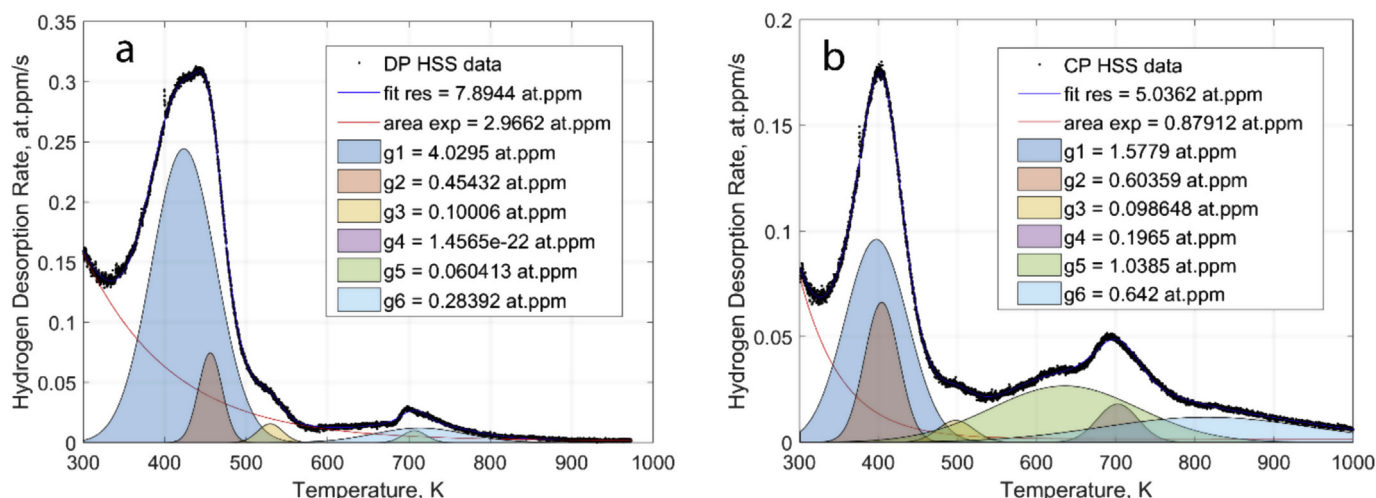


Fig. 5. Fitting of the TDS curves of DP (a) and CP (b) steels after fatigue loading until fracture. The goodness of fitting is 0.98 and 0.97 for DP and CP steels, respectively.

shown in yellow with red boundaries. The amount of RA in the as-supplied sample of the DP steel was estimated from the EBSD data to be about 0.25%, while the CP steel contains about 0.92%. The retained austenite mean size of a few tens of nanometers are distributed preferably at grain boundaries and interphases in both studied steels. However, the CP steel contains also the RA with the size of a few hundred nanometers which forms on the grain boundaries as well as inside of grains. After fatigue loading, the content of the RA decreases in both steels as shown in Fig. 7c and d. The content of the RA was calculated from the EBSD data to be about 0.09% and 0.46% in DP and CP steels, respectively. The results differ significantly as compared to that obtained from magnetic measurement [3]. The difference is apparently caused by RA phase etching during steel polishing in colloidal silica. However, EBSD phase mapping is sufficient for a comparative analysis of RA phase content before and after fatigue testing. The length of α/γ interfaces was measured from Fig. 7 and found to be about 45 μm in DP steel and 79 μm in CP steel before fatigue testing. After fatigue fracture the interface length decreases to about 16 μm and 30 μm , respectively. Worth to note is the variation of the RA volume fraction is more remarkable than the RA interface area between DP and CP steels. Since the CP steel contains the retained austenite phase inclusions with a wide range of size, the analysis of its distribution was performed as

shown in Fig. 8. RA size distribution calculated for the as-supplied state was compared to that after fatigue fracture evidencing a significant reduction of austenite content with a mean size of about 100 nm after the fatigue loading.

A significant increase of the crystal lattice distortion density forming as a result of fatigue loading was observed in both studied steels and shown in Fig. 9. Volume fraction of the distorted areas after fatigue loading was increased at about 25% and 8% in DP steel and CP steel, respectively.

Micrographs of the fatigue crack initiation zone in both steels are shown in Fig. 10a and b. Fatigue crack was initiated transgranularly in both studied steels, while the CP steel contains also intergranular fracture areas as shown in Fig. 10b. The DP steel has a well-defined quasi-cleavage area starting from the side surface of the specimen. With the increase of the fatigue crack length the fracture morphology changes from transgranular to the dimple ductile fracture.

4. Discussion

The hydrogen concentration increase observed in both studied steels after fatigue loading evidences the hydrogen uptake from the air environment during the test. Under the fatigue loading hydrogen uptake

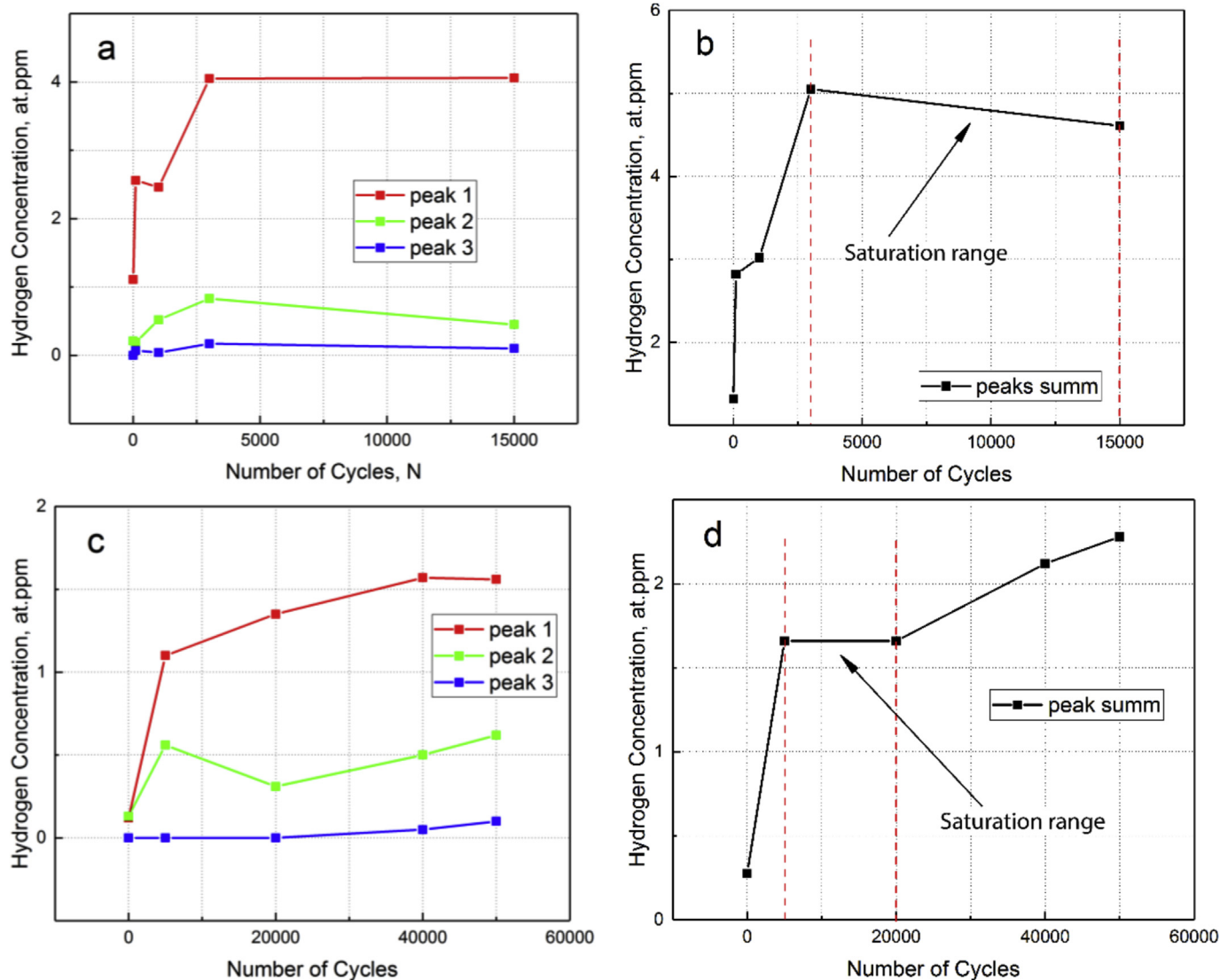


Fig. 6. Hydrogen concentration as a function of a number of fatigue cycles calculated from the fitting data separately for each peak of the low-temperature component (a, c) and its sum (b, d) for DP (a, b) and CP (c, d) steels.

and diffusion into the steel may occur in a few steps:

1. Air contains some amount of water vapor that forms moisture on the specimen surface;
2. The oxidation reaction of the bare metal surface results in the formation of so-called corrosion-generated hydrogen [15,18], part of which enters into the specimen bulk. With the increase of temperature the reaction of oxidation is enhanced, resulting in an increase of hydrogen generation;
3. The chemisorption of hydrogen results in its following diffusion from the surface to the interstitial sites of the metal crystal lattice, grain boundaries, NMI interfaces, etc. [19].

The oxide layer formed on the specimen surface suppresses further ingress of hydrogen into the steel. However, applied fatigue loading results in the oxide layer cracking caused by persisted slip bands formation, which produce facets of bare metal and oxidation with hydrogen uptake continues.

The observed complex hydrogen thermal desorption spectra are related to the microstructure of the studied steels. The low-temperature component consists of three well-defined peaks, which correspond to certain hydrogen trapping sites (see Fig. 5). The increase of the

hydrogen concentration observed after fatigue loading is accompanied by the growth of the low-temperature component of the thermal desorption spectra, but it is not the case for the high-temperature component. One can assume that the high-temperature component of the hydrogen desorption spectra is associated with decomposition of the molecular hydrogen trapped in voids and/or bubbles during the metallurgical processes. The assumption needs, however, further investigation.

Fig. 6b, d shows that the concentration of hydrogen in both steels increases steeply during the first 3000–5000 cycles approaching the saturation. Then the total concentration of hydrogen remains nearly constant until 15 000–20 000 cycles forming the range of saturation. The separate analysis of the peaks (see Fig. 6a, c) evidences that the hydrogen concentration which corresponds to peaks 1 and 2 increases together during the initial stage of the fatigue testing in both steels. The hydrogen concentration of peak 2 decreases, however, during the saturation range in both steels, while the hydrogen concentration of peak 1 increases slowly. The concentration of hydrogen corresponding to peak 3 increases just slightly and remains almost the same during the saturation range for DP steel. In the CP steel, hydrogen concentration of the peak 3 starts to increase after the saturation range up to the end of the fatigue life.

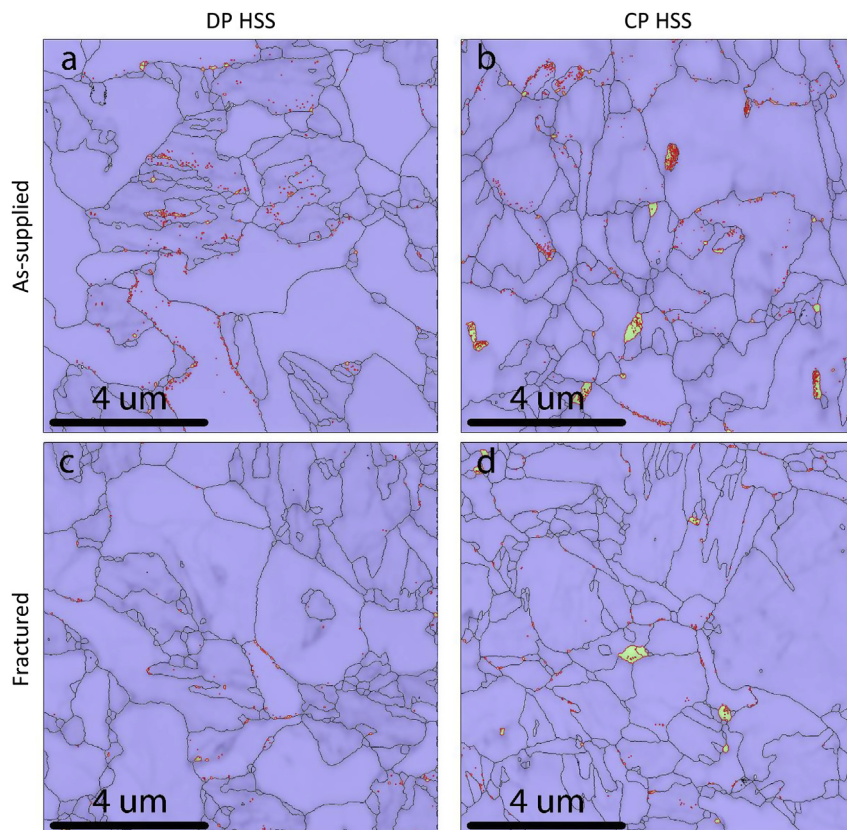


Fig. 7. Phase contrast micrograph of DP (a, c) and CP (b, d) HSS grades obtained from the specimens in as-supplied conditions (a, b) and after fatigue fracture (c, d).

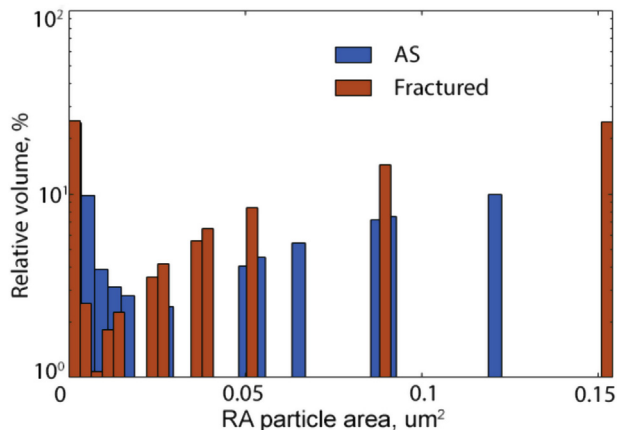


Fig. 8. Grain size distribution of the retained austenite phase inclusions calculated for CP steel in as-supplied condition and after fatigue fracture.

The peak 1 contains the major part of the trapped hydrogen and reflects, probably, hydrogen trapping by the crystal lattice defects forming in the course of the fatigue loading as shown in Fig. 9. The volume fraction of the lattice distortions caused by the defects was increased by about 25% in DP steel and 8% in CP steel following with hydrogen concentration increases to about 4 at ppm and 1.5 at ppm, respectively (see Fig. 6). The observed reduction of the hydrogen concentration, which corresponds to the peak 2, is apparently associated with a reduction of the retained austenite due to its transformation to martensitic phase taking place in the course of the fatigue loading (see Fig. 7) [10,20]. The amount of the retained austenite decreases by about 2 times after the fatigue loading to fracture. Phase transformation preferably occurs in the RA with a size of less than about 100 nm, which are distributed preferably on the grain boundaries and interfaces as

shown in Fig. 7. However, peak 2 is not apparently directly related to the hydrogen trapping by the retained austenite bulk. One can assume that the trapping sites are probably located at the interface between the RA and matrix. This hypothesis is supported by the fact that α/γ interface area differs by less than two times in DP and CP steels, while the difference of the RA volume fraction is much more significant. At the same time, the hydrogen concentration which corresponds to peak 2 differs slightly between DP and CP steels. The similar phenomenon was observed previously by Chan et al. [9], who proposed the mechanism of hydrogen diffusion retardation by the fine-film retained austenite between the martensitic plates that support the present results.

DP steel specimens were fractured after about 15 000 cycles at the end of the saturation range of the hydrogen uptake. But, the hydrogen concentration in CP steel starts to increase again after about 20 000 cycles (see Fig. 6d), which is probably related to the attenuation of the RA transformation rate. The observed continuous increase of the hydrogen concentration is preferably caused by hydrogen trapping associated with peak 2 and peak 3. In other words, the total hydrogen concentration in the CP steel increases due to the hydrogen trapping at the α/γ interfaces.

One can assume that peak 3 relates to the hydrogen desorption from the retained austenite bulk due to the relatively high temperature of hydrogen desorption compared to the peaks 1 and 2. The temperature position of peak 3 correlates well with what was observed in metastable austenitic AISI 301LN stainless steel [21]. A minor variation of hydrogen thermal desorption peaks temperature in DP and CP steels is apparently caused by variation of the chemical composition of RA in both steels. At the same time, peak 3 appears as a precursor of the fatigue fracture in both steels. One can also assume that additional trapping sites with a stronger affinity to hydrogen may form at RA interfaces under applied fatigue loading [22]. Trapping sites in the form of vacancies or vacancy complexes are accumulated at the phase boundaries and stabilized by hydrogen [23].

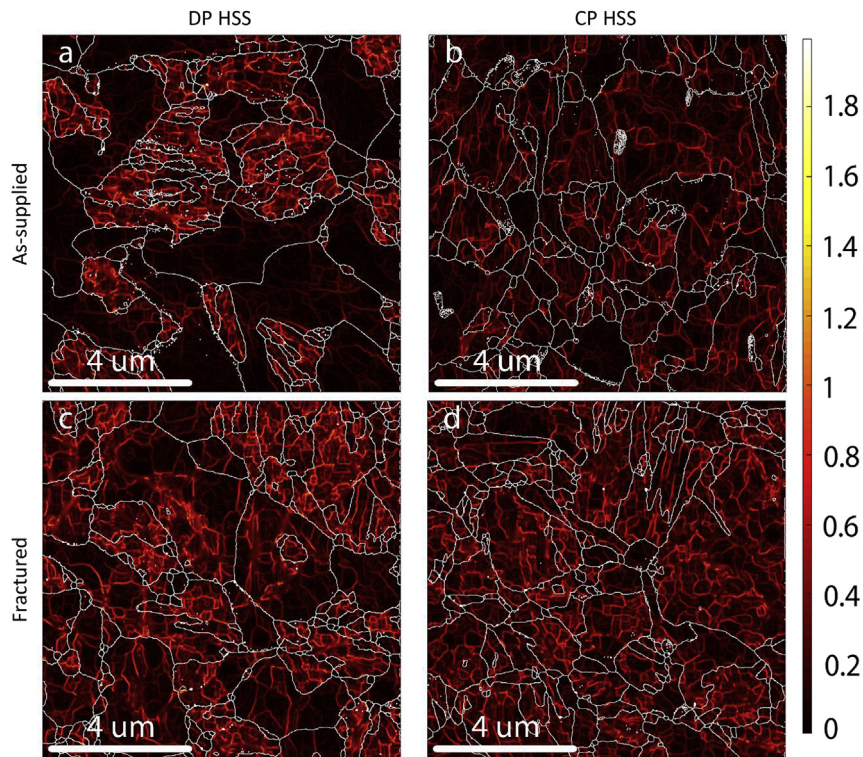


Fig. 9. Kernel misorientation map of DP (a, c) and CP (b, d) HSS grades obtained from the specimens in as-supplied conditions (a, b) and after fatigue fracture (c, d).

Fractography evidences a different mechanism of the fatigue crack initiation in DP and CP steels. Fatigue crack was initiated by cleavage in DP steel starting from the side surface of the specimen as shown in Fig. 10a. Cleavage crack probably originates from the plastic-deformation process, since the applied fatigue load is close to the offset yield point of the DP steel as shown in Fig. 2 [24]. The morphology of the fracture surface changes from cleavage to transgranular fatigue crack propagation accompanied by the formation of striations and secondary cracks. Secondary cracks are apparently associated with hydrogen-induced decohesion at the α'/γ interface [7,25]. Fatigue crack initiation in the CP steel is preferably transgranular but contains also the intergranular fracture zones with the size of about 5 μm distributed close to the side surfaces of the specimen (about 100–200 μm from the side surface). The observed intergranular fracture areas might be formed due to hydrogen accumulation at the α'/γ interfaces and following hydrogen-induced decohesion. Fatigue crack was apparently initiated from the observed intergranular fracture areas. One can conclude that hydrogen trapping at the interfaces between the retained austenite and matrix causes the hydrogen-assisted fracture rather than hydrogen trapping in the retained austenite bulk. A possible mechanism of the hydrogen-induced fatigue fracture in high strength steel is schematically shown in Fig. 11. Moisture on the specimen surface results in oxidation/corrosion reaction that is followed by water

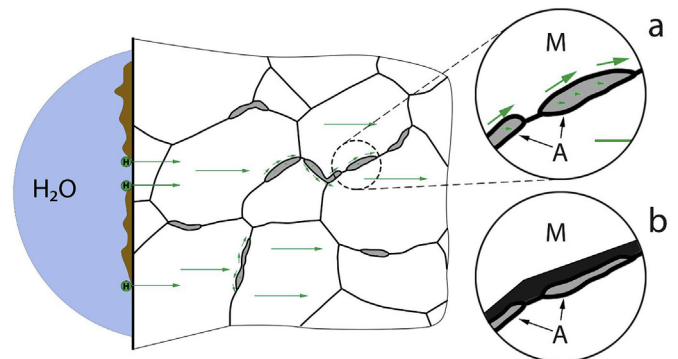


Fig. 11. Schematic diagram showing the hydrogen uptake and diffusion (a) leading to intergranular fracture (b) in the studied high-strength steel during fatigue loading. The length of the green arrows shows schematically the diffusion rate of hydrogen. Hydrogen accumulated at the interface of the thin film retained austenite inclusions results in intergranular fracture due to hydrogen-enhanced decohesion at the α'/γ interface. Martensitic and austenitic phases are defined as M and A, respectively. (For interpretation of the references to colour in this figure legend, the reader is referred to the Web version of this article.)

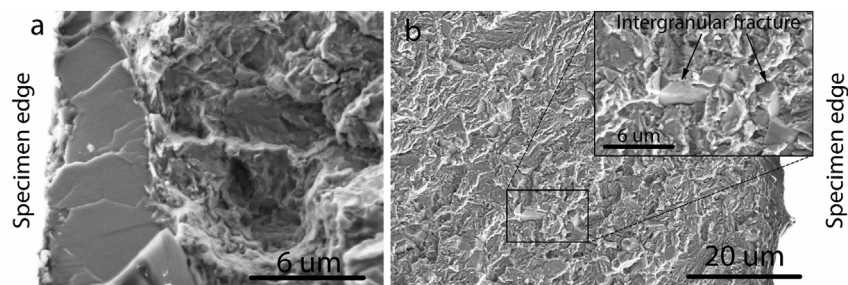


Fig. 10. Fatigue crack initiation zone of the DP (a) and CP (b) steel specimens. The insert shows details of the intergranular fracture.

decomposition and hydrogen chemisorption on the specimen surface. The absorbed hydrogen diffuses into the bulk of the steel, where it comes along the interfaces of the retained austenite. The diffusion of hydrogen atoms at the interfaces is retarded as proposed by Chan et al. [9].

In the presence of the external loading, the hydrogen accumulated at the interfaces causes nucleation of the hydrogen-assisted crack due to the hydrogen-induced decohesion mechanism [25]. Solheim et al. have shown a significant effect of retained austenite amount on the ductility of super-martensitic stainless steel tested in presence of hydrogen [10]. The major effect, however, appears to be caused by the increased amount of interfaces between the retained austenite and matrix rather than by the increased volume fraction of the retained austenite.

5. Conclusions

The concentration of hydrogen in the studied DP and CP high-strength steels increases with fatigue loading time in the air.

Fatigue loading results in a significant reduction of the retained austenite amount caused by its transformation to the martensitic phase.

Fatigue crack propagates transgranularly in both DP and CP high strength steels. Fatigue crack is initiated by cleavage in DP steel due to an excess of plastic deformation during the test, while in CP steel the fatigue crack is initiated from the intergranular fracture areas, which is often observed in the vicinity of the side surface of the specimen.

Analysis of the hydrogen trapping and microstructure changes of the steels evidence that hydrogen becomes trapped at the interfaces between the thin-film retained austenite and matrix rather than in retained austenite bulk. Hydrogen trapping at the α'/γ interfaces most likely results in intergranular fatigue crack initiation in HSS under fatigue loading.

Data availability

The raw/processed data required to reproduce these findings cannot be shared at this time as the data also forms part of an ongoing study.

Acknowledgments

The research was supported by the post-doctoral scholarship no. 9155273 Aalto University School of Engineering, Department of Mechanical Engineering, Finland.

References

- [1] J.P. Hirth, Effects of hydrogen on the properties of iron and steel, *Metall. Trans.* 11A (1985) 861–890.
- [2] S. Takagi, Y. Toji, M. Yoshino, K. Hasegawa, Hydrogen embrittlement resistance evaluation of ultra-high strength steel sheets for automobiles”, *ISIJ Int.* 52 (2012) 316–322.
- [3] T. Hicckel, R. Nazarov, E. McEniry, Z. Zermout, Y. Yagodzinsky, H. Hanninen, O. Rott, R. Thiessen, K. Mrachek, Hydrogen Sensitivity of Different Advanced High Strength Microstructures (HYDROMICROS), European Commission, Final report, 978-92-79-45820-0, 2015, <https://doi.org/10.2777/07315>.
- [4] Y. Murakami, N.N. Yokoyama, K. Takai, Effect of hydrogen trapped by inclusions on ultra-long life fatigue failure of bearing steel, *J. Soc. Mater. Sci.* 50 (2001) 1068–1073.
- [5] O. Todoshchenko, Y. Yagodzinsky, V. Yagodzinska, T. Saukkonen, H. Hanninen, Hydrogen effects on fracture of high-strength steels with different micro-alloying, *Corros. Rev.* 33 (2015) 515–527.
- [6] K.V. Sudhakar, E.S. Dwarakadasa, A study on fatigue crack growth in dual phase martensitic steel in air environment, *Bull. Mater. Sci.* 23 (2000) 193–199.
- [7] I.H. Onn, N. Ahmad, M.N. Tamin, “Fatigue characteristics of dual phase steel sheets”, *J. Mech. Sci. Technol.* 29 (2014) 51–57.
- [8] K.S. Ravichandran, E.S. Dwarakadasa, K. Kishore, Some consideration on the occurrence of intergranular fracture during fatigue crack growth in steels, *Mater. Sci. Eng.* 83 (1986) L11–L16.
- [9] S.L.I. Chan, H.L. Lee, J.R. Yang, Effect of retained austenite on the hydrogen content and effective diffusivity of martensitic structure, *Metall. Trans. A* 22 (1991) 2579–2586.
- [10] K.G. Solheim, J.K. Solberg, J. Walmsley, F. Rosenqvist, T.H. Bjørnå, The role of retained austenite in hydrogen embrittlement of supermartensitic stainless steel, *Eng. Fail. Anal.* 34 (2013) 140–149.
- [11] R.A. McCoy, W.W. Gerberich, V.F. Zackay, On the resistance of TRIP steel to hydrogen embrittlement, *Metall. Mater. Trans. B* 1 (1970) 2031–2034.
- [12] E.D. Cabanillas, L. Terminiello, N.A. Cantalejos, R. Versaci, R.C. Mercader, Mössbauer studies of strain-induced transformation of retained austenite in dual-phase steels, *Mater. Sci. Eng. A* 150 (1992) 113–116.
- [13] T. Sakai, M. Ramulu, M. Suzuki, Temperature and humidity effects on fatigue life distribution of carbon steel, *Int. J. Fatigue* 13 (1991) 117–125.
- [14] Y.H. Zhang, Review of the Effect of Hydrogen Gas on the Fatigue Performance of Steels, Paper Presented at 29th International Conference on Offshore Mechanics and Arctic Engineering (OMAE 2010), 2010 Shanghai, China, 6–11 June.
- [15] L. Gao, B.E. Conway, Adsorption and desorption of hydrogen into the hydrogen evolution reaction and the effect of co-adsorbed poisons, *Electrochem. Acta* 39 (1994) 1681–1693.
- [16] G.W. Hong, J.Y. Lee, The measurement of the trap binding energy by the thermal analysis, *Scripta Metall.* 17 (1983) 823–826.
- [17] S.W. Smith, J.R. Scully, The identification of hydrogen trapping states in an Al-Li-Cu-Zn alloy using thermal desorption spectroscopy, *Metall. Mater. Trans. A* 31 (2000) 179–193.
- [18] B.E. Wilde, C.D. Kim, Hydrogen adsorption on steels undergoing corrosion with hydrogen evolution, *Corrosion* 42 (1986) 243–244.
- [19] M.R. Shanabarger, A. Taslami, H.G. Nelson, Influence of hydrogen chemisorption kinetics on the interpretation of hydrogen transport through iron membranes, *Scripta Metall.* 15 (1981) 929–933.
- [20] E. Folkhard, *Welding Metallurgy of Stainless Steels*, (1984) 978-3-7091-8965-8 Wien New York.
- [21] Y. Yagodzinsky, O. Todoshchenko, S. Papula, H. Hanninen, Hydrogen solubility and diffusion in austenitic stainless steels studied with thermal desorption spectroscopy”, *Steel Res. Int.* 82 (2011) 20–25.
- [22] Y. Yagodzinsky, S. Papula, H. Hanninen, Role of the internal hydrogen in delayed cracking of metastable low-Ni austenitic stainless steels, *Proceedings of the Third International Conference on Metals and Hydrogen*, 2018.
- [23] M.G. Ganchenkova, Y.N. Yagodzinsky, V.A. Borodin, H. Hanninen, Effects of hydrogen ind impurities on void nucleation in copper: simulation point of view, *Phil. Mag.* 94 (2014) 3522–3548.
- [24] R.E. Reed-Hill, *Physical Metallurgy Principles*, third ed., PWS Publishing Company, Boston, 0-534-92173-6, 1991.
- [25] S.P. Lynch, Hydrogen embrittlement phenomena and mechanisms, *Corros. Rev.* 30 (2012) 105–123.